Acta Mechanica Solida Sinica, Vol. 25, No. 6, December, 2012 ISSN 0894-9166
Published by AMSS Press, Wuhan, China

FEM ANALYSIS FOR INFLUENCES OF A FAULT ON COUPLED T-H-M-M PROCESS IN DUAL-POROSITY ROCK MASS**

Yujun Zhang[1]* **Chaoshuai Yang**[2] **Gang Xu**[1]

([1] *State Key Laboratory of Geomechanics and Geotechnical Engineering, Institute of Rock and Soil Mechanics, The Chinese Academy of Sciences, Wuhan* 430071, *China*)

([2] *Technology Centre, China Railway Tunnel Group Co. Ltd, Luoyang* 471009, *China*)

Received 5 November 2010, revision received 9 September 2011

ABSTRACT For the case in which a large geological structure like fault existing within the surrounding rock mass in the near field of a repository for high-level radioactive nuclear waste, one kind of coupled thermo-hydro-mechanical-migratory model of dual-porosity medium for saturated-unsaturated ubiquitous-joint rock mass was established. In the present model, the seepage field and the concentration field are double, but the stress field and the temperature field are single, and the influences of sets, spaces, angles, continuity ratios, stiffness of fractures on the constitutive relationship of the medium can be considered. At the same time, a two-dimensional program of finite element method was developed. Taking a hypothetical nuclear waste repository located at a rock mass being unsaturated dual-porosity medium as a calculation example, the FEM analysis for thermo-hydro-mechanical-migratory coupling were carried out under the condition of radioactive nuclide leaking for the cases with and without a fault, and the temperatures, pore pressures, flow velocities, nuclide concentrations and principal stresses in the rock mass were investigated. The results show that the fracture water in the fault flows is basically along the fault direction, and its flow velocity is almost three orders of magnitude higher than that of fracture water in rock mass; the nuclide concentration in the fault is also much higher than that without fault, and the nuclides move along the fault faster; moreover, the fault has obvious influences on the pore pressures and the principal stresses in the rock mass.

KEY WORDS fault, dual-porosity medium, thermo-hydro-mechanical-migratory coupling, FEM analysis

I. INTRODUCTION

Some countries like China, Japan, Sweden, Switzerland and Canada plan to carry out geological disposal for high-level radioactive nuclear waste in granite body while the United States of America will perform it in tuff[1, 2]. As a natural barrier preventing the nuclides from releasing out, the granite and tuff have some advantages including large scale of rock mass, high mechanical strength, good thermal conductivity and stability, good absorbability and retardation capability of radioactive nuclide and so on; but they also have some distributed joints and fractures with variable lengths and densities which promote

* Corresponding author. E-mail: yjzhang@whrsm.ac.cn

** Project supported by the National Key Basic Research and Development Program of China (973 Project) (No. 2010CB732101), the National Natural Science Foundation of China (No. 51079145), and the Research Fund of State Key Laboratory of Geomechanics and Geotechnical Engineering (No. SKLQ008).

flow of groundwater[3]. One of the key problems concerned with the high-level radioactive geological disposal waste is how harmful nuclides migrate with the groundwater flowing, if they can enter into the biosphere and how to retard them, etc. Therefore, it is important to establish a mathematical model for the discontinuity (joints, fractures, faults, etc.) and to research thermo-hydro-mechanical-chemical coupling[4–6].

According to the porosity and fracture, rock mass can be dealt with either a homogeneous medium or dual-media. For the former in which the sporadic joints and fractures are distributed, several joint models were put forward considering the thermo-hydro-mechanical coupling, such as the models of Noorishad's[7], the Nguyen's[8], the Tijani's[9], and the authors' plane model as well as three-dimension model[10, 11]. For the later, because of the ubiquitous joint and fracture, the joint-element does not exist any longer independently, but fracture medium is used to simulate the ubiquitous joint, such as the models of Ling Bing's[12], Olivella's[13], Rutqvist's[14]. On the basis of existing research results, the constitutive model for thermo-hydro-mechanical-migratory coupling process in dual-porosity media is put forward, and a relative two dimensional elastic-plastic FEM program is developed by the first author, which has been used to carry out a numerical simulation for the ubiquitous-jointed rock mass rather than for the rock mass distributed sparse discontinuous geological structures with large thickness.

In this paper, taking a hypothetical nuclear waste repository located at a rock mass being unsaturated dual-porosity medium, we carried out the FEM analysis for thermo-hydro-mechanical-migratory coupling under a certain initial conditions of temperature, pore pressures, flow velocities of groundwater, radioactive nuclide leaking for the cases with and without a fault (loose and broken, highly permeable) in surrounding rock. And we investigate the distributions and changes of temperatures, pore pressures, flow velocities, nuclide concentrations and principal stresses in the rock mass as well as the impact of fault, and obtain some conclusions.

II. THERMO-HYDRO-MECHANICAL-MIGRATORY COUPLING EQUATIONS FOR DUAL-POROSITY MEDIA

For the dual-porosity medium it can be assumed that the temperature field and the stress field being single, but there exist pore water pressure and fracture water pressure, pore concentration and fracture concentration, and the groundwater and solute can be exchanged due to the pressure and concentration differences existing between fracture and porosity. So a two dimensional model for coupled thermo-hydro-mechanical-migratory process is created. The governing equations are given as follows:

2.1. Stress Equilibrium Equation

Supposing there are n sets of fractures in a fractured porous rock mass, we can write the stress equilibrium equation in the global coordinate system as

$$\frac{\mathrm{d}\boldsymbol{\sigma}}{\mathrm{d}t} = \boldsymbol{D}\left[\frac{\mathrm{d}\boldsymbol{\varepsilon}}{\mathrm{d}t} - \boldsymbol{m}\left(\boldsymbol{C}_1 - \frac{1}{3K_s}\right)(s_{w1} + D_{s1}p_{w1})\frac{\mathrm{d}p_{w1}}{\mathrm{d}t} - \boldsymbol{m}\left(\boldsymbol{C}_2 - \frac{1}{3K_s}\right) \times (s_{w2} + D_{s2}p_{w2})\frac{\mathrm{d}p_{w2}}{\mathrm{d}t} - \boldsymbol{m}\frac{\beta_S}{3}\frac{\mathrm{d}T}{\mathrm{d}t}\right] \tag{1}$$

where $\boldsymbol{\sigma}$ and $\boldsymbol{\varepsilon}$ are the total stress and total stain, respectively, $\boldsymbol{D} = (\boldsymbol{C}_1 + \boldsymbol{C}_2)^{-1}$ is the elastic matrix, $\boldsymbol{m}^{\mathrm{T}} = \{1\,1\,0\}$ is the unit normal column matrix, K_s, β_S, T are the bulk modulus, synthesized thermal expansion coefficient and temperature of the fractured porous rock mass, respectively, s_{w1}, p_{w1}, D_{s1}, $\boldsymbol{C}_1$ and s_{w2}, p_{w2}, D_{s2}, $\boldsymbol{C}_2$ are the saturation degree, water pressure, specific moisture content and flexibility matrix of rock matrix and fractured network, respectively, and t is the time.

2.2. Continuity Equation for Groundwater

On the basis of the principle of mass balance, the water volume flowing into an object during a time increment of $\mathrm{d}t$ is equal to the rate of water accumulation within the object. Assuming that the seepage of water can be expressed by Darcy law, the continuity equation for rock matrix is expressed by

$$-\nabla^{\mathrm{T}}\left\{\boldsymbol{k}_1\frac{k_{rw1}}{\mu_w}\nabla(p_{w1} + \gamma_w z)\right\} + \frac{\bar{\alpha}\boldsymbol{k}_1 k_{rw1}}{\mu_w}(p_{w1} - p_{w2}) + \boldsymbol{A}_1\frac{\partial\boldsymbol{\varepsilon}}{\partial t} + \boldsymbol{B}_1\frac{\partial p_{w1}}{\partial t} + \boldsymbol{E}_1\frac{\partial p_{w2}}{\partial t} + \boldsymbol{F}_1\frac{\partial T}{\partial t} - \nabla^{\mathrm{T}}D_{t1}\nabla T = 0 \tag{2}$$

where $\boldsymbol{k}_1$ and k_{rw1} are the intrinsic permeability tensor and relative permeability of rock matrix, respectively, ρ_w, μ_w and γ_w are the density of water, dynamic viscosity of water and unit weight of water, respectively, z is the head above some arbitrary datum, $\bar{\alpha}$ is a coefficient which depends on the fracture width and geometry, D_{t1} is the thermal water diffusivity of rock matrix, and $\boldsymbol{A}_1$, $\boldsymbol{B}_1$, $\boldsymbol{E}_1$ and $\boldsymbol{F}_1$ are all the constant matrixes.

For the fractured system, the continuity equation can be derived in a similar way as follows:

$$-\nabla^{\mathrm{T}}\left\{\boldsymbol{k}_2\frac{k_{rw2}}{\mu_w}\nabla(p_{w2}+\gamma_w z)\right\}+\frac{\bar{\alpha}\boldsymbol{k}_1 k_{rw1}}{\mu_w}(p_{w1}-p_{w2})$$
$$+\boldsymbol{A}_2\frac{\partial\boldsymbol{\varepsilon}}{\partial t}+\boldsymbol{B}_2\frac{\partial p_{w2}}{\partial t}+\boldsymbol{E}_2\frac{\partial p_{w1}}{\partial t}+\boldsymbol{F}_2\frac{\partial T}{\partial t}-\nabla^{\mathrm{T}}D_{t2}\nabla T=0 \tag{3}$$

where $\boldsymbol{k}_2$ and k_{rw2} are the intrinsic permeability tensor and relative permeability of fractured medium, respectively; $\boldsymbol{A}_2$, $\boldsymbol{B}_2$, $\boldsymbol{E}_2$ and $\boldsymbol{F}_2$ can be obtained by replacing subscripts 1 and 2 in expressions of $\boldsymbol{A}_1$, $\boldsymbol{B}_1$, $\boldsymbol{E}_1$ and $\boldsymbol{F}_1$ with subscripts 2 and 1.

2.3. Energy Conservation Equation

In accordance with the principle of energy conservation, the rate of heat inflow into an object equals the increase of the internal energy within the object. The temperature field is thought to be single. The energy conservation equation takes the form

$$-\nabla^{\mathrm{T}}\boldsymbol{\lambda}\nabla T+(s_{w1}\phi_1\boldsymbol{V}_1^a+s_{w2}\phi_2\boldsymbol{V}_2^a)\rho_w C_w(\nabla^{\mathrm{T}}T)+\left[(1-\phi_1)C_sT\frac{\rho_s}{K_s}+\phi_1C_wT\frac{\rho_w}{K_w}\right](s_{w1}+D_{s1}p_{w1})$$
$$\times\frac{\partial p_{w1}}{\partial t}-\{(1-\phi_1)C_sT\rho_s\beta_s+(\phi_1+\phi_2)C_wT\rho_w\beta_w-[(1-\phi_1)\rho_sC_s+(\phi_1+\phi_2)\rho_wC_w]\}\frac{\partial T}{\partial t}$$
$$+\frac{1}{2}(1-\phi_1)\beta_sT\frac{\partial}{\partial t}(u_{i,j}+u_{j,i})\delta_{ij}=0 \tag{4}$$

where C_w is the specific heat of water, C_s, ρ_s and $\boldsymbol{\lambda}$ are the specific heat, density and thermal conductivity matrix of fractured porous rock mass, respectively; $\boldsymbol{V}_1^a$ and $\boldsymbol{V}_2^a$ are the apparent flow velocities of pore water and fracture water, respectively; u_i and u_j are the displacement components; and δ_{ij} is the Kronecker's delta.

2.4. Percolation-Migration Equation

The Percolation-migration equation for the homogeneous medium in Ref.[15] was improved by the author with the new interpretation of adding the solute exchange between rock matrix and fractured network due to concentration difference, which made it suitable for the dual-porosity media. The new percolation-migration equation is derived from the old one as follows:

$$R_i\theta_i\rho_w\frac{\partial c_i}{\partial t}=\nabla^{\mathrm{T}}\theta_i\rho_w\boldsymbol{D}_i\nabla c_i-\theta_i\rho_w\boldsymbol{V}_i\nabla c_i-R_i\theta_i\rho_w\chi c_i+(-1)^{i+1}\bar{\omega}\theta_i\rho_w\boldsymbol{D}_1(c_1-c_2)-Q_{ci} \tag{5}$$

where $i=1,2$, correspond to rock matrix and fractured network, respectively, R_i is the retardation coefficient and is defined as $R_i=\dfrac{V_i}{V_i^*}=\left(1+\dfrac{\rho_{di}}{\theta_i}K_{di}\right)$, V_i is the apparent velocity of groundwater, V_i^* is the transport velocity of radioactive nuclide, ρ_{di} is the dry density of rock matrix or fractured network, K_{di} is the distribution coefficient for saturated media, θ_i is the volumetric water content, ρ_w is the water density, $\boldsymbol{D}_i$ is the diffusion tensor, c_i is the concentration of solute, $\boldsymbol{V}_i$ determined by the coupled of temperature, seepage and stress is the apparent velocity vector of groundwater, χ is the radioactive decay constant, $\bar{\omega}$ is the coefficient which depends on the fracture width and geometry, and Q_{ci} is the source term.

The diffusion tensor can be given by

$$D_{i\alpha\beta}=\alpha_{i\mathrm{T}}|V_i|\delta_{\alpha\beta}+(\alpha_{i\mathrm{L}}-\alpha_{i\mathrm{T}})\frac{V_{i\alpha}V_{i\beta}}{|V_i|}+\alpha_{i\mathrm{m}}\tau_i\delta_{\alpha\beta} \tag{6}$$

where $\alpha_{i\mathrm{T}}$ is the dispersivity in the transversal direction, $\alpha_{i\mathrm{L}}$ is the dispersivity in the longitudinal direction, $|V_i|$ is the absolute value of the apparent flow velocity, $\alpha_{i\mathrm{m}}$ is the molecular diffusion coefficient, τ_i is the tortuosity coefficient, and $\delta_{\alpha\beta}$ is the Kronecker's delta.

III. ESTABLISHING FEM PATTERN

3.1. Discretization in Space Domain

By means of Galerkin method, the finite element discretization in the space domain is carried out for the equilibrium equation, the continuity equation, the energy conservation equation and the percolation-migration equation. The system of semi-discrete coupled formulae is yielded as follows after regulation:

$$\begin{aligned}
&\boldsymbol{K}\frac{\mathrm{d}\bar{\boldsymbol{u}}}{\mathrm{d}t}+\boldsymbol{C}\frac{\mathrm{d}\bar{p}_{w1}}{\mathrm{d}t}+\boldsymbol{I}\frac{\mathrm{d}\bar{p}_{w2}}{\mathrm{d}t}+\boldsymbol{J}\frac{\mathrm{d}\bar{T}}{\mathrm{d}t}=\frac{\mathrm{d}\boldsymbol{f}}{\mathrm{d}t}\\
&\boldsymbol{E}_1\frac{\mathrm{d}\bar{\boldsymbol{u}}}{\mathrm{d}t}+\boldsymbol{G}_1\frac{\mathrm{d}\bar{p}_{w1}}{\mathrm{d}t}+\boldsymbol{H}_1\frac{\mathrm{d}\bar{p}_{w2}}{\mathrm{d}t}+\boldsymbol{F}_1\bar{p}_{w1}+\boldsymbol{M}\bar{p}_{w1}-\boldsymbol{M}\bar{p}_{w2}+\boldsymbol{U}_1\bar{T}+\boldsymbol{V}_1\frac{\mathrm{d}\bar{T}}{\mathrm{d}t}=\boldsymbol{0}\\
&\boldsymbol{E}_2\frac{\mathrm{d}\bar{\boldsymbol{u}}}{\mathrm{d}t}+\boldsymbol{G}_2\frac{\mathrm{d}\bar{p}_{w1}}{\mathrm{d}t}+\boldsymbol{H}_2\frac{\mathrm{d}\bar{p}_{w2}}{\mathrm{d}t}+\boldsymbol{F}_2\bar{p}_{w2}-\boldsymbol{M}\bar{p}_{w1}+\boldsymbol{M}\bar{p}_{w2}+\boldsymbol{U}_2\bar{T}+\boldsymbol{V}_2\frac{\mathrm{d}\bar{T}}{\mathrm{d}t}=\boldsymbol{X}\\
&\boldsymbol{A}\frac{\mathrm{d}\bar{\boldsymbol{u}}}{\mathrm{d}t}+\boldsymbol{P}\frac{\mathrm{d}\bar{p}_{w1}}{\mathrm{d}t}+\boldsymbol{R}\bar{T}+\boldsymbol{Q}\frac{\mathrm{d}\bar{T}}{\mathrm{d}t}=\boldsymbol{Y}\\
&\boldsymbol{W}_1\bar{c}_1+\boldsymbol{L}_1\frac{\mathrm{d}\bar{c}_1}{\mathrm{d}t}+\boldsymbol{S}\bar{c}_1-\boldsymbol{S}\bar{c}_2=\boldsymbol{0}\\
&\boldsymbol{W}_2\bar{c}_2+\boldsymbol{L}_2\frac{\mathrm{d}\bar{c}_2}{\mathrm{d}t}+\boldsymbol{S}\bar{c}_2-\boldsymbol{S}\bar{c}_1=\boldsymbol{Z}
\end{aligned}\tag{7}$$

where $\bar{\boldsymbol{u}}$, $\bar{p}_{w1}$, $\bar{p}_{w2}$, $\bar{T}$, $\bar{c}_1$ and $\bar{c}_2$ are the unknown variables, in which the bold-faced capital letters stand for constant matrixes; $\boldsymbol{f}$ is the column matrix of external force due to boundary and body force loadings; $\boldsymbol{X}$, $\boldsymbol{Y}$ and $\boldsymbol{Z}$ are the column matrixes of water loading, heat loading and solute concentration loading owing to existence of source term and boundary outflow term, respectively.

3.2. Discretization in Time Domain

Using the monolithic augmentation approach, $\bar{\boldsymbol{u}}$, $\bar{p}_{w1}$, $\bar{p}_{w2}$, $\bar{T}$, $\bar{c}_1$ and $\bar{c}_2$ are approximated with a linear variation within each time step Δt, and $\bar{c}_1$, $\bar{c}_2$ can be decoupled with other variables. So Eq.(7) become the following Equations with a step-by-step method:

$$\begin{aligned}
&\begin{bmatrix}
\boldsymbol{K} & \boldsymbol{G} & \boldsymbol{I} & \boldsymbol{J}\\
\boldsymbol{E}_1 & \boldsymbol{G}_1+\eta(\boldsymbol{F}_1+\boldsymbol{M})\Delta t_k & \boldsymbol{H}_1-\eta\boldsymbol{M}\Delta t_k & \boldsymbol{V}_1+\eta\boldsymbol{U}_1\Delta t_k\\
\boldsymbol{E}_2 & \boldsymbol{G}_2-\eta\boldsymbol{M}\Delta t_k & \boldsymbol{H}_2+\eta(\boldsymbol{F}_2+\boldsymbol{M})\Delta t_k & \boldsymbol{V}_2+\eta\boldsymbol{U}_2\Delta t_k\\
\boldsymbol{A} & \boldsymbol{P} & \boldsymbol{0} & \boldsymbol{Q}+\eta\boldsymbol{R}\Delta t_k
\end{bmatrix}_{t,\eta}
\begin{Bmatrix}\bar{\boldsymbol{U}}\\ \bar{P}_{w1}\\ \bar{P}_{w2}\\ \bar{T}\end{Bmatrix}_{t_k+\Delta t_k}\\
&\quad=\begin{bmatrix}
\boldsymbol{K} & \boldsymbol{G} & \boldsymbol{I} & \boldsymbol{J}\\
\boldsymbol{E}_1 & \boldsymbol{G}_1-(1-\eta)(\boldsymbol{F}_1+\boldsymbol{M})\Delta t_k & \boldsymbol{H}_1+(1-\eta)\boldsymbol{M}\Delta t_k & \boldsymbol{V}_1-(1-\eta)\boldsymbol{U}_1\Delta t_k\\
\boldsymbol{E}_2 & \boldsymbol{G}_2+(1+\eta)\boldsymbol{M}\Delta t_k & \boldsymbol{H}_2-(1-\eta)(\boldsymbol{F}_2+\boldsymbol{M})\Delta t_k & \boldsymbol{V}_2-(1-\eta)\boldsymbol{U}_2\Delta t_k\\
\boldsymbol{A} & \boldsymbol{P} & \boldsymbol{0} & \boldsymbol{Q}-(1-\eta)\boldsymbol{R}\Delta t_k
\end{bmatrix}_{t,\eta}\\
&\qquad\cdot\begin{Bmatrix}\bar{\boldsymbol{U}}\\ \bar{P}_{w1}\\ \bar{P}_{w2}\\ \bar{T}\end{Bmatrix}_{t_k}+\begin{Bmatrix}\dfrac{\partial\boldsymbol{f}}{\partial t}\\ \boldsymbol{0}\\ \boldsymbol{X}\\ \boldsymbol{Y}\end{Bmatrix}_{t,\eta}\Delta t_k
\end{aligned}\tag{8}$$

$$\begin{aligned}
&\begin{bmatrix}
\boldsymbol{L}_1+\eta(\boldsymbol{W}_1+\boldsymbol{S})\Delta t_k & -\eta\boldsymbol{S}\Delta t_k\\
-\eta\boldsymbol{S}\Delta t_k & \boldsymbol{L}_2+\eta(\boldsymbol{W}_2+\boldsymbol{S})\Delta t_k
\end{bmatrix}_{t,\eta}
\begin{Bmatrix}\bar{c}_1\\ \bar{c}_2\end{Bmatrix}_{t_k+\Delta t_k}\\
&\quad=\begin{bmatrix}
\boldsymbol{L}_1-(1-\eta)(\boldsymbol{W}_1+\boldsymbol{S})\Delta t_k & (1+\eta)\boldsymbol{S}\Delta t_k\\
(1+\eta)\boldsymbol{S}\Delta t_k & \boldsymbol{L}_2-(1-\eta)(\boldsymbol{W}_2+\boldsymbol{S})\Delta t_k
\end{bmatrix}_{t,\eta}
\begin{Bmatrix}\bar{c}_1\\ \bar{c}_2\end{Bmatrix}_{t_k}+\begin{Bmatrix}\boldsymbol{0}\\ \boldsymbol{Z}\end{Bmatrix}_{t,\eta}\Delta t_k
\end{aligned}\tag{9}$$

IV. VERIFICATION OF COUPLING MODEL FOR DUAL-POROSITY MEDIA

For the above-mentioned thermo-hydro-mechanical-migratory coupling model of the dual-porosity media, a two-dimensional FEM code is developed here. The rationality of the model and code is verified as follows.

Because there is no analytic solution for thermo-hydro-mechanical-migratory coupling up to now, and it is difficult to find the suitable in-situ test data for simulation at this time, we try to utilize existing

Table 1. **Column coefficients**

Young's modulus E (MPa)	1.0
Poisson's ratio μ	0.15
Fissure stiffness k_n (MPa/m)	0.1
Fluid bulk modulus k_f (MPa)	0.1
Matrix porosity ϕ_1	0.1
Fissure porosity ϕ_2	0.05
Matrix permeability k_1/μ (m^2/Pa.s)	0.01×10^{-9}
Fissure permeability k_2/μ (m^2/Pa.s)	0.1×10^{-6}
Fissure spacing S (m)	0.1

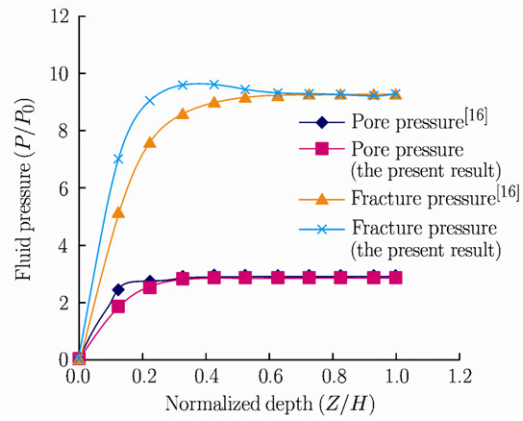

Fig. 1. Pore pressure equilibration responses for column at 4000 s.

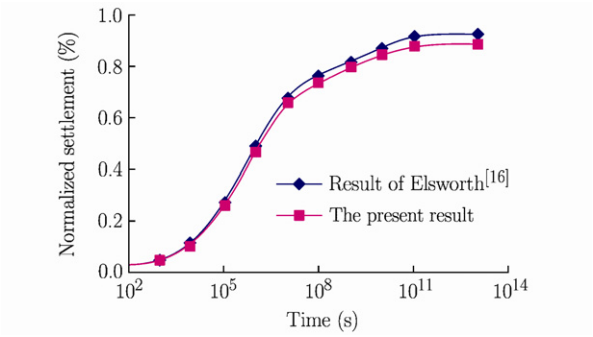

Fig. 2. Surface settlements versus time for column.

numerical solution to verify the model. Elsworth put forward a coupled hydro-mechanical model for dual-porosity media. As an examination example it is assumed that a well-distributed loading P_0 is applied on the top of a one-dimensional saturated column with a fracture spacing of 0.1 m, and the hydrologic-mechanical properties of material are reported in Table 1. A numerical simulation of hydro-mechanical coupling for the column was executed by using the relative FEM software. In order to compare the coupled thermo-hydro-mechanical-migratory model with Elsworth's model, an FEM analysis of hydro-mechanical coupling for the same column, in which the temperature is a constant and the solute migration is not considered temporarily, was also made using our code. The fluid pressure responses with the depth of the column obtained by Elsworth and authors are illustrated in Fig.1, and the corresponding surface settlement associated with the expulsion of fluid from the dual-porosity system is represented in Fig.2. It can be seen from these figures that the simulation results by two computation programs are very close, indicating that our model is reliable.

V. COMPUTATION EXAMPLE

As shown in Fig.3, it is assumed that a canister filled with the vitrified radioactive nuclear waste is disposed at the depth of 1000 m beneath the ground surface. As an approximate simplification, it is treated to be a plane strain problem. A computational region with a horizontal length of 4 m and a vertical length of 8 m is taken. There are 800 elements and 861 nodes in the mesh. From the margin of the vitrified waste, the node numbers are 432, 433, 434, 435, 436, respectively. The rock mass is an unsaturated medium, in which there exist one set of horizontal fracture and two sets of vertical fracture which are orthogonal, and there is a horizontal fault with width of 0.4 m in the middle part of computational region. Referring to the rock mass situations of DST test performed at Yucca Mountain in USA[17], the relative calculating parameters are presented in Tables 2 and 3.

The porous rock mass has high water content, but the fractured network is quite dry. The initial saturations of the rock matrix and fracture system are 0.9, 0.1 and 0.2 respectively, and their water

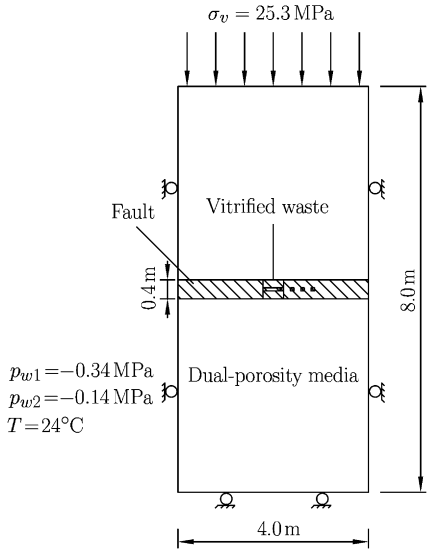

Fig. 3. Computation model.

retention curves conform to the Van Genuchten model, that is

$$s_w = (s_{ws} - s_{wr})(1 + |\alpha\psi|^n)^{-m} + s_{wr} \tag{10}$$

where α, n and $m = 1 - 1/n$ are the material constants, ψ is the water potential head, s_{ws} and s_{wr} are the maximum saturation and the minimum saturation, respectively. For the rock matrix, $\alpha = 2.25 \times 10^{-6}$ m^{-1}, $n = 1.33$, s_{ws}, s_{wr} are 1.0 and 0.18, respectively, so the initial pore pressure in rock matrix is -0.34 MPa; for the fracture system, $\alpha = 9.74 \times 10^{-5}$ m^{-1}, $n = 1.97$, s_{ws}, s_{wr} are 1.0 and 0.01, respectively, so the initial pore pressure in fracture system is -0.14 MPa.

Table 2. **Main computation parameters for rock and vitrified waste*****

media	ρ	ϕ_1	k_1/μ_w	E (MPa)	μ	C	β	λ
Rock mass	25.3	0.11	1.24×10^{-10}	1.48×10^{4}	0.21	0.95	1.0×10^{-6}	2.0
Fault	23.0	0.3	1.24×10^{-8}	1.48×10^{2}	0.21	0.95	1.0×10^{-6}	2.0
Vitrified waster	25.0	0.0	1.0×10^{-27}	5.3×10^{4}	0.21	0.7	1.0×10^{-6}	5.3

***ρ(kN· m^{-3}): the density; ϕ_1: the porosity; k_1/μ_w(m^2/Pa·s): the permeability;
C(kJ·kg^{-1}·°C^{-1}): the specific heat; β(°C^{-1}): the thermal Expan. Coeff.;
λ(W·m^{-1}·°C^{-1}): the thermal conductivity.

Table 3. **Parameters for fracture sets used in calculation**

Parameter	Fracture set	
	Horizontal fracture	Vertical fracture
Spacing, S(m)	0.3	0.3
Continuity ratio, l	1	1
Dip angle, θ (°)	0	90
Normal stiffness, k_n(MPa/m)	2000.0	1000.0
Shearing stiffness, k_s(MPa/m)	1000.0	500.0
Porosity, ϕ_2	0.01	0.01
Constant, $\bar{\alpha}$ (m^{-2})	0.01	0.01
Permeability of rockmass, k_2/μ_w(m^2/Pa·s)	1.0×10^{-6}	1.0×10^{-6}
Permeability of fault, k_2/μ_w(m^2/Pa·s)	1.0×10^{-2}	1.0×10^{-2}

The relationship between relative permeability and saturation degree is

$$k_{rw} = s_w^{2.0} \tag{11}$$

The thermal water diffusivities of both the rock matrix and fracture system are taken as

$$D_t = 2.0 \times 10^{-11}\,\mathrm{m}^2/(\mathrm{s}\cdot^\circ\mathrm{C}) \tag{12}$$

The boundary conditions are as follows: The free displacement, the fixed temperature and pore water pressure are allowed for the top of computational domain on which the vertical stress is applied due to the overburden load. Both left and right sides with fixed horizontal displacement, are adiabatic and impermeable. The vertical displacement, temperature and pore water pressure are fixed at the bottom surface. The temperature of rock mass and buffer is uniform, with a value of 20.0°C at the initial stage. It is supposed that after finishing embedding of a waste canister, the canister is damaged by some reasons, so that the radioactive nuclides begin to leak out into the near field with a constant concentration and rate from the canister. The time when the nuclides begin to leak out is taken as the start time of the computation. The temperature in the computation domain is 24°C (uniformly distributed). The vitrified waste is the source term with a diffusive mass flux of radioactive nuclides $Q_c = 1.44\times10^{-8}\mathrm{mol\cdot kg/m^3\cdot s^{-1}}$. The constants used in the computation concerned with the percolation-migration of nuclide are supposed as follows: The tortuosity coefficients τ_1, τ_2 are 0.4 and 0.8, respectively; the dispersivities in the longitudinal direction $\alpha_{1\mathrm{L}}$ and $\alpha_{2\mathrm{L}}$ are 1.0 m and 2.0 m, respectively; the dispersivities in the transversal direction are $\alpha_{i\mathrm{T}} = \alpha_{i\mathrm{L}}/10$, the molecular diffusion coefficients $\alpha_{1\mathrm{m}}$ and $\alpha_{2\mathrm{m}}$ are 1.0×10^{-9} m^2/s and 2.0×10^{-9} m^2/s, respectively; the distribution coefficients K_{d1} and K_{d2} are 8.0 ml/g and 5.3 ml/g, respectively; the dry densities ρ_{d1} and ρ_{d2} are 23.0 kg/m^3 and 21.0 kg/m^3, respectively; the parameter $\bar{\omega}$ is 100.0 m^{-2}; the radioactive decay constant $\chi = \ln 2$ Thalf, where Thalf is the half life of the nuclide which is taken as 1000 years in the computation. The waste radiates continuously heat with a power of 300 W during a period of 4 years, and the time step is taken as 100000 s.

For the case with and without a fault (which named case 1 and case 2 for short, respectively), the author studied the distributions and changes of temperatures, pore pressures, flow velocities, nuclide concentrations and principal stresses in the rock mass. The main computation results and analysis are as follows.

The temperature fields of two cases are almost the same, which shows that the fault has less influence on the temperature field. Taking case 1 for instance, the temperatures versus time at the nodes 432, 433, 434, 435 in Fig.3 are shown in Fig.4. In the early 0.15 a, the temperature of buffer increases fast,

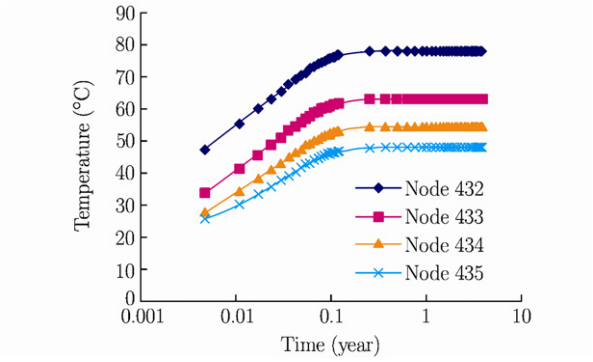

Fig. 4. Temperatures versus time at some nodes.

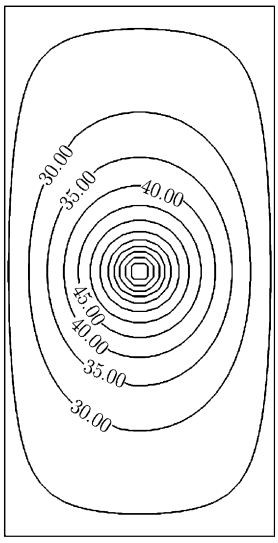

Fig. 5. Contour plots of temperature in calculation domain at 4 years (°C).

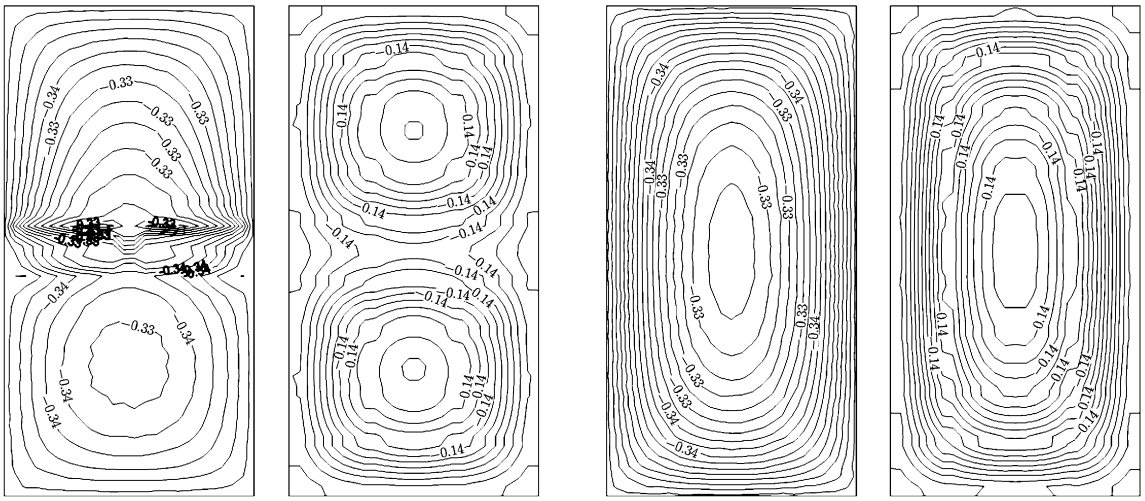

Fig. 6. Contour plots of pore water pressure in the buffer at 4 years (MPa).

and then it grows slowly. At the termination of computation, the temperatures of nodes 432,433,434 and 435 are 77.9 °C, 63.1°C, 54.4°C and 48.0°C, respectively. Contour plots of temperature in the calculation domain at 4 years are shown in Fig.5.

Figure 6 shows the contours of pore pressure and fracture pressure at 4 a in the computation region, from which it can be seen that for the case with and without a fault, it is significant to distinguish the pore pressure from the fracture pressure, especially in vicinity of the fault, but the difference between them is not large. Taking the node 433 for instance, the pore pressure and the fracture pressure at the end of computation are −0.334 MPa, −0.137 MPa for case 1 and −0.333 MPa, −0.138 MPa for case 2, respectively.

Figure 7 shows the flow velocity vectors of pore and fracture for case 1 and case 2 at 4 a. The scales of these two kinds of vectors are different—1:10 for case 1 and 1:2 for case 2, respectively. It is seen that for case 1 not only the flow velocities of pore and fracture in the fault are higher than that in the corresponding section, but also the fracture water flows along with the fault, and the velocity

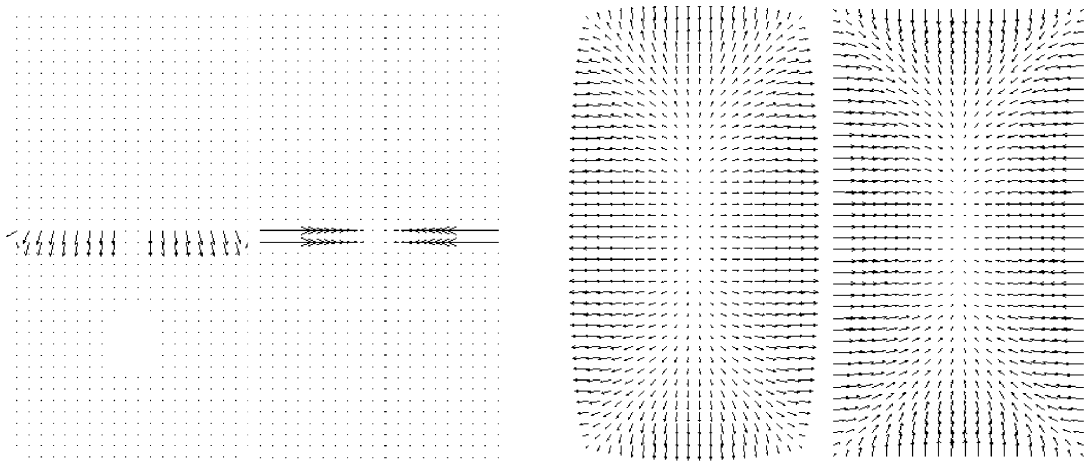

Fig. 7. Flow velocity vectors in near field of disposal repository at 4 years.

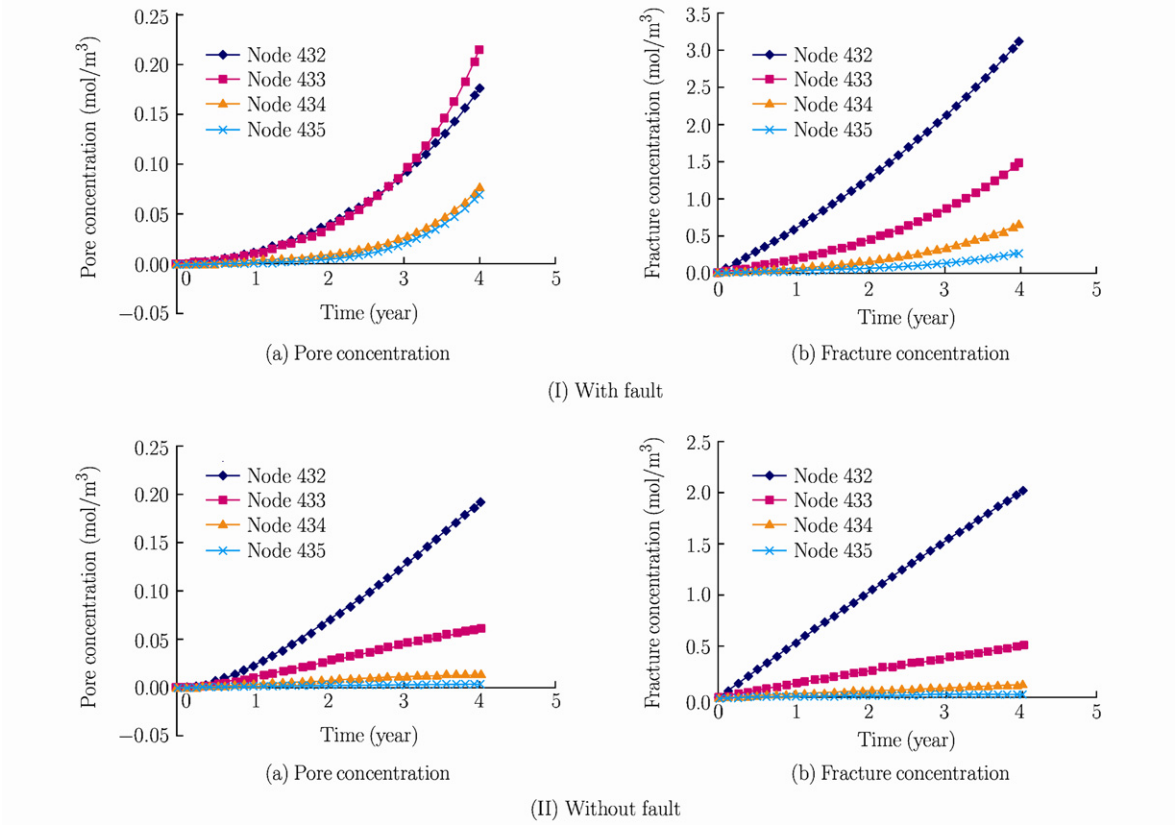

Fig. 8. Nuclide concentrations versus time at some nodes.

fields for the two cases display great difference. Taking the node 432 for instance, the pore velocity and the fracture velocity at 4 a are 1.18×10^{-3}m/s, 2.41×10^{-5}m/s for case 1 and 4.90×10^{-8}m/s, 5.28×10^{-8}m/s for case 2, respectively. It is shown that the velocity of pore with a low permeability coefficient is higher than that of fracture with a large one in the fault for case 1 and the velocity in pore is close to that in fracture. The principle reason is that the initial saturations of pore and fracture are different—0.9 and 0.1, respectively, so the relative permeability of the former is great larger than that of the later. Meanwhile, temperature effect causes those two kinds of groundwater pressures to change differently, making the flow velocity of pore higher (for case 1) or slightly lower (for case 2) than that of fracture in this special condition.

The pore and fracture nuclide concentrations of nodes 432, 433, 434, 435 versus time for the two cases are plotted in Fig.8. It can be seen that the nuclides concentrations of both pore and fracture in the fault for case 1 non-linearly rise with acceleration, and the former value is about 1/10 of the later one. It indicates that although a great number of nuclide migrates along the fracture channels, a certain amount of nuclide still diffuses in pores. However, in the corresponding section for case 2 they increase non-linearly with a deceleration (in spite of a slight extent) and the former value is only about 1/1000 of the later one, which also shows that a great number of nuclide migrates along the fracture channels in the rack mass and the nuclide concentration of pore is low. Taking the node 432 for instance, the nuclide concentrations of pore and fracture at 4 a are 3.11 mol/m^3, 0.18 mol/m^3 for case 1 and 2.01 mol/m^3, 1.82×10^{-4} mol/m^3 for case 2, respectively. The nuclide concentrations of pore and fracture in the site of fault for case 1 are muck higher than that in the corresponding location for case 2. The contours of nuclide concentrations of pore and fracture within the range of 2 m×2 m around the canister at 4a are shown in Fig.9, from which it can be seen that the nuclides migrate faster along the fault direction.

Principal stress contours in near field of disposal repository for two cases at 4 a are shown in Fig.10, from which it can be seen that there exists stress concentration in and near the fault for case 1, so that the distribution and value of principle stress in this area are quite different from that for case 2.

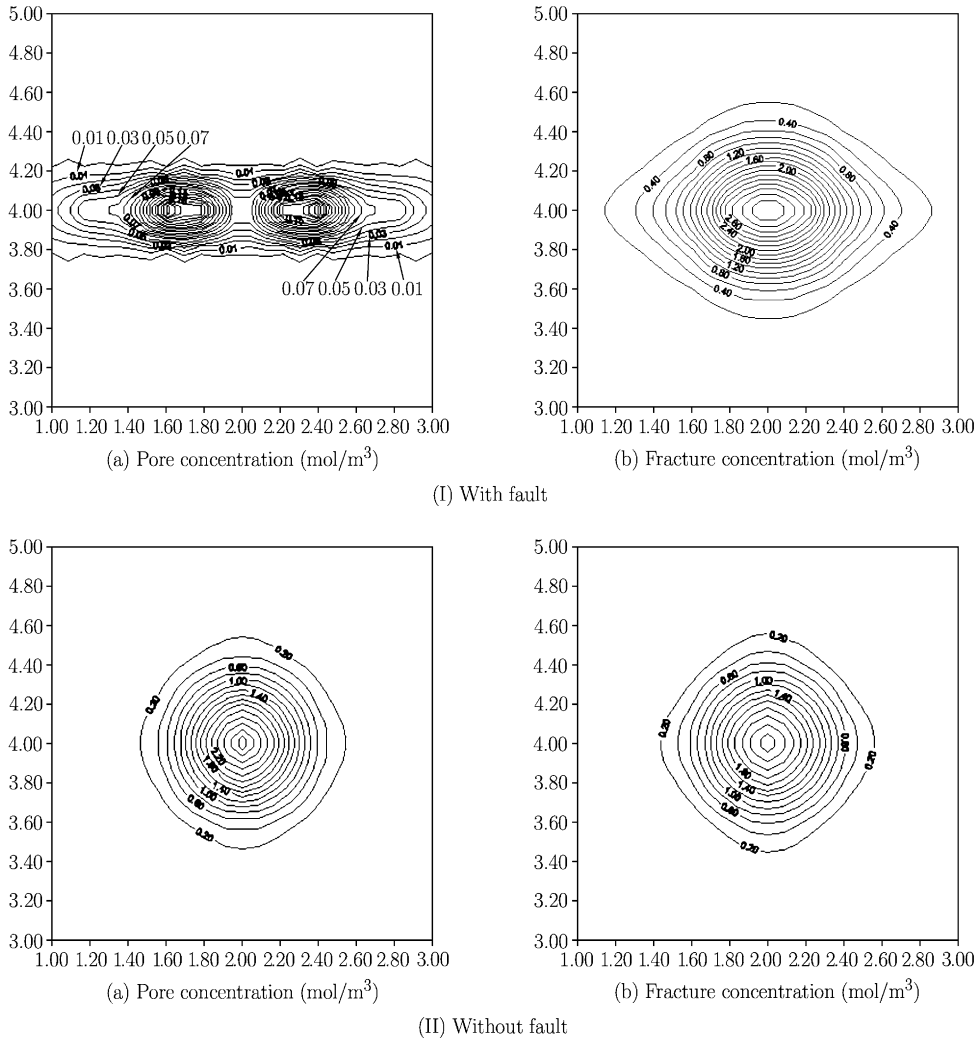

Fig. 9. Contour plots of nuclide concentrations at 4 years.

However, the principal stress in the upper and the lower sections from the fault much further away from the positions in those two cases have little difference. The max/min main stress of nodes 432, 433, 434, 435 are $-4.2/-17.2$ MPa, $-3.8/-20.9$ MPa, $-4.2/-21.9$ MPa, $-4.5/-22.5$ MPa for case 1 and $4.9/-18.4$ MPa, $2.5/-18.9$ MPa, $0.8/-19.4$ MPa, $-0.48/-19.8$ MPa for case 2, respectively. In comparison with the rock mass without a fault, the absolute value of minimum principal stress (compressive) becomes large in the fault located in the corresponding site of surrounding rock, and the maximum principal stress is changed from less 'compressive' or 'tensile' of surrounding rock without a fault into higher 'compressive' or 'compressive' for case with a fault, since the elastic modulus in the fault is only 1/100 of that in rock mass.

VI. CONCLUDING REMARKS

For the saturated-unsaturated ubiquitous-joint rock mass, the influences of sets, spaces, angles, continuity ratios, stiffness of fractures on the constitutive relationship of the medium can be considered and the fields of both stress and temperature are single. The groundwater and the nuclides can be exchanged due to the pressure and concentration differences existing between fracture and porosity. So a 2D model coupled thermo-hydro-mechanical-migratory for dual-porosity medium was established, and the relative three-dimensional code of finite element method was developed.

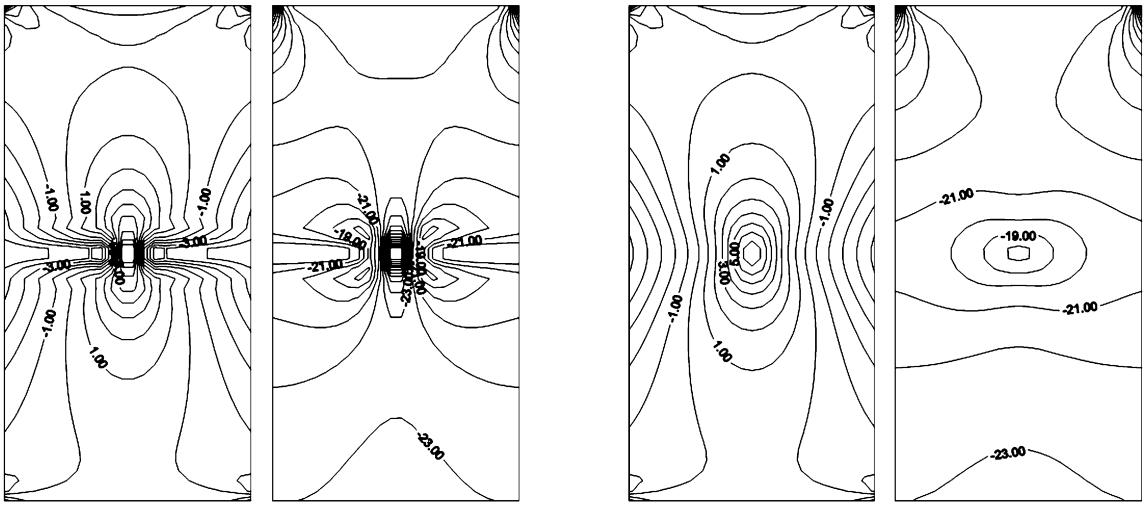

Fig. 10. Contour plots of principal stresses in near field of disposal repository at 4 years (MPa).

Taking a hypothetical nuclear waste repository located at a rock mass being unsaturated dual-porosity medium as a calculation example, the numerical simulation for thermo-hydro-mechanical-migratory coupling was carried out under the condition of radioactive nuclide leaking for the cases with and without a horizontal fault traversing the canister. The computation results showed that the temperatures in the near field of the repository rise rapidly during 0.15 a at the beginning, then change quite little, at the end of computation (4.0 a) where it can reach 30.0-80.0°C in the near field. For the case with and without a fault, it is significant to distinguish the pore pressure from the fracture pressure in the vicinity of the fault position, but the value of the former is close to that of the later. And the fracture water in the fault flows basically along the fault direction, and its flow velocity is almost three orders of magnitude higher than that of the fracture water in rock mass; The nuclides concentrations of both pore and fracture in the fault non-linearly rise with acceleration while in the corresponding section for case without a fault they increase non-linearly with a deceleration (in spite of a little extent), and the nuclide concentration in the fault is also much higher than that in the corresponding part without fault. Although the nuclides mainly migrate by the fracture channels for the case with or without a fault, the nuclides move along the fault faster. In comparison with the rock mass without a fault, there exists stress concentration in and near the fault. The absolute value of compressive principal stress becomes large while tensile principal stress is changed into the compressive one.

For the fault in the dual-porosity surrounding rock where a geological disposal repository for high-level radioactive nuclear waste is located, not only the process of thermo-hydro-mechanical-migratory coupling is strongly influenced due to the large permeability coefficient, low elastic modulus and strength, but also it will act as a passage of the nuclides leaking out into the biosphere. Therefore, this possible case must be studied sufficiently.

References

[1] Wang,J., Zheng,H.L., Xu,G.Q., Fan,X.H., Wang,C.Z. and Fan,Z.W., Geological disposal of high level radioactive waste in China: progress in last decade (1991-2000). In: Wang Ju, Fan Xianhua, Xu Guoaing, Zheng Hualing, editors, Geological Disposal of High Level Radioactive Waste in China: Progress in Last Decade. Beijing: Atomic Energy Press, 2004: 1-12 (in Chinese).

[2] TRW Environmental Safety Systems Inc., Drift Scale Test Progress Report No.1. Las Vegas: TRW Environmental Safety Systems Inc., 1998.

[3] Min,M.Z. and Xu,G.Q., Principles for Disposal of Radioactive Waste. Beijing: Atomic Energy Press, 1998 (in Chinese).

[4] Ohnishi,Y., Chan,T. and Jing,L., Constitutive models for rock joins. In: Stephansson,O., Jing,L., Tsang,C.-F., eds. Coupled Thermo-Hydro-Mechanical Processes of Fractured Media, Vol. 79. Elsevier: Development in Geotechnical Engineering, 1996: 57-91.

[5] Rutqvist,J., Chijimatsu,M., Jing,L., Millard,A., Nguyen,T.S., Rejeb,A., Sugita,Y. and Tsang,C.F., Anumerical study of THM effects on the near-field safety of a hypothetical nuclear waste repository—BMT1 of the DECOVALEX III project. Part 3: Effects of THM coupling in sparsely fractured rocks. *International Journal of Rock Mechanics and Mining Sciences*, 2005, 42(5-6): 745-755.

[6] Jing,L.R. and Feng,X.T., Main rock mechanics issures in geological disposal of radioactive wastes. *Chinese Journal of Rock Mechanics and Engineering*, 2006, 25(4): 833-841 (in Chinese).

[7] Noorishad,J. and Tsang,C.F., Coupled thermohydroelasticity phenomena in variably saturated fractured porous rocks—Formulation and numerical solution. In: Stephansson,O., Jing,L. and Tsang,C.-F. editor, Coupled Thermo-Hydro-Mechanical Progresses of Fractured Media, 79, Elsevier: Development in Geotechnical Engineering, 1996, 93-134.

[8] Nguyen,T.S., Description of the computer code FRACON. In: Stephansson,O., Jing,L. and Tsang,C.-F. editor, Coupled Thermo-Hydro-Mechanical Progresses of Fractured Media, 79, Elsevier: Development in Geotechnical Engineering, 1996: 539-544.

[9] Tijani,S.-M. and Vouille,G., FEM analysis of coupled THM processes in fractured media with explicit representation of joints. In: Stephansson,O., Jing,L. and Tsang,C.-F. editor, Coupled Thermo-Hydro-Mechanical Progresses of Fractured Media, 79, Elsevier: Development in Geotechnical Engineering, 1996: 165-180.

[10] Zhang,Y.J., A kind of joint element simulating coupled thermo-hydro-mechanical phenomenon and relevant numerical analyses. *Chinese Journal of Geotechnical Engineering*, 2005, 27(3): 270-274 (in Chinese).

[11] Zhang,Y.J., 3D joint element and relevant numerical analysis simulating coupled thermo-hydro-mechanical processes. *Chinese Journal of Geotechnical Engineering*, 2009, 31(8): 1213-1218 (in Chinese).

[12] Liang,B., Liu,L., Xue,Q. and Sun,W.J., Study on numerical simulation of nuclides leakage for groundwater pollution. *Journal of System Simulation*, 2007, 19(2): 261-311 (in Chinese).

[13] Olivella,S. and Gens,A., Double structure THM analyses of a heating test in a fractured tuff incorporating intrinsic permeability variations. *International Journal of Rock Mechanics and Mining Sciences*, 2005, 42(5/6): 667-679.

[14] Rutqvis,J. and Tsang,C.-F., Analysis of thermal-hydrologic-mechanical behavior near an emplacement drift at Yucca mountain. *Journal of Contaminant Hydrology*, 2003, 62-63: 637-652.

[15] Nishigaki,M., Density Dependent Transport Analysis Saturateds-Unsaturated Porous Media—3 Dimensional Eulerian Lagrangian Method. Okayama University, 2001.

[16] Elsworth,D. and Mao,B., Flow-deformation response of dual-porosity media. *Journal of Geotechnical Engineering*, 1992, 118(1): 107-124.

[17] Rutqvist,J., Barr,D., Datta,R., Gens,A., Millard,A., Olivella,S., Tsang,C.-F. and Tsang,Y., Coupled thermal-hydrological-mechanical analyses of the Yucca Mountain Drift Scale Test—Comparison of field measurements to predictions of four different numerical models. *International Journal of Rock Mechanics and Mining Sciences*, 2005, 42(5/6): 680-697.